

Pulsed-source spectral-domain optical coherence tomography with reduced motion artifacts

S. H. Yun, G. J. Tearney, J. F. de Boer, and B. E. Bouma

*Harvard Medical School and Wellman Center of Photomedicine,
Massachusetts General Hospital
50 Blossom Street, BAR-718, Boston, Massachusetts 02114
syun@hms.harvard.edu*

Abstract: We demonstrate a novel technique based on pulsed light sources for spectral domain optical coherence tomography. The use of short optical pulses enables the acquisition of axial profiles of a sample with an effective integration time much less than the reciprocal of the camera readout rate thereby greatly reducing motion artifacts. We also show that motion-induced signal fading can be avoided by using a wavelength-swept source.

©2004 Optical Society of America

OCIS codes: (110.4500) Optical coherence tomography; (170.3880) Medical and biological imaging

References and links

1. A.F. Fercher, C. K. Hitzenberger, G. Kamp, S. Y. El-Zaiat, "Measurement of intraocular distances by backscattering spectral interferometry," *Opt. Comm.* **117**, 43-48 (1995).
2. G. Hausler and M. W. Lindner, "Coherence radar and spectral radar - new tools for dermatological diagnosis," *J. Biomed. Opt.* **3**, 21-31 (1998).
3. P. Andretzky, M. W. Lindner, J. M. Herrmann, A. Schultz, M. Konzog, F. Kieseletter, and G. Hausler, "Optical coherence tomography by spectral radar: dynamic range estimation and in vivo measurements of skin," *Proc. SPIE* **3567**, 78-87 (1998).
4. M. Wojtkowski, A. Kowalczyk, R. Leitgeb, and A. F. Fercher, "Full range complex spectral optical coherence tomography technique in eye imaging," *Opt. Lett.* **27**, 1415-1417 (2002).
5. M. Wojtkowski, T. Bajraszewski, P. Targowski, and A. Kowalczyk, "Real time in vivo imaging by high-speed spectral optical coherence tomography," *Opt. Lett.* **28**, 1745-1747 (2003).
6. N. Nassif, B. Cense, B. H. Park, S. H. Yun, T. C. Chen, B. E. Bouma, G. J. Tearney, and J. F. de Boer, "In vivo human retinal imaging by ultrahigh-speed spectral domain optical coherence tomography," *Opt. Lett.* **29**, 480-482 (2004).
7. S. H. Yun, G. J. Tearney, B. E. Bouma, B. H. Park, and J. F. de Boer, "High-speed spectral domain optical coherence tomography at 1.3 μm wavelength," *Opt. Express* **11**, 3598-3604 (2003).
8. N. Nassif, B. Cense, B. H. Park, S. H. Yun, G. J. Tearney, B. E. Bouma, T. C. Chen, and J. F. de Boer, "In vivo high-resolution video-rate spectral-domain optical coherence tomography of the human retina and optic nerve," *Opt. Express* **12**, 367-376 (2004).
9. R. A. Leitgeb, W. Drexler, A. Unterhuber, B. Hermann, T. Bajraszewski, T. Le, A. Stingl, and A. F. Fercher, "Ultrahigh resolution Fourier domain optical coherence tomography," *Opt. Express* **12**, 2156-2165 (2004),
<http://www.opticsexpress.org/abstract.cfm?URI=OPEX-12-10-2156>
10. B. Cense, N. A. Nassif, T. C. Chen, M. C. Pierce, S. Yun, B. H. Park, B. E. Bouma, G. J. Tearney, and J. F. de Boer, "Ultrahigh-resolution high-speed retinal imaging using spectral-domain optical coherence tomography," *Opt. Express* **12**, 2435-2447 (2004),
<http://www.opticsexpress.org/abstract.cfm?URI=OPEX-12-11-2435>
11. M. Wojtkowski, V. J. Srinivasan, T. H. Ko, J. G. Fujimoto, A. Kowalczyk, and J. S. Duker, "Ultrahigh-resolution, high-speed, Fourier domain optical coherence tomography and methods for dispersion compensation," *Opt. Express* **12**, 2404-2422 (2004),
<http://www.opticsexpress.org/abstract.cfm?URI=OPEX-12-11-2404>
12. S. H. Yun, G. J. Tearney, J. F. de Boer, and B. E. Bouma, "Motion artifacts in optical coherence tomography with frequency domain ranging," *Opt. Express* **12**, 2977-2998 (2004),
<http://www.opticsexpress.org/abstract.cfm?URI=OPEX-12-13-2977>

13. S. H. Yun, G. J. Tearney, J. F. de Boer, N. Iftimia, and B. E. Bouma, "High-speed optical frequency-domain imaging," *Opt. Express* **11**, 2953-2963 (2003), <http://www.opticsexpress.org/abstract.cfm?URI=OPEX-11-22-2953>
 14. S. H. Yun, C. Boudoux, G. J. Tearney, and B. E. Bouma, "High-speed wavelength-swept semiconductor laser with a polygon-scanner-based wavelength filter," *Opt. Lett.* **28**, 1981-1983 (2003).
 15. B. E. A. Saleh and M. C. Teich, *Fundamental of photonics*, ch 14 (John Wiley & Sons, New York, 1991)
 16. S. V. Chernikov, Y. Zhu, J. R. Taylor, and V. P. Gapontsev, "Supercontinuum self-Q-switched ytterbium fiber laser," *Opt. Lett.* **22**, 298-300 (1997).
 17. W. J. Wadsworth, N. Joly, J. C. Knight, T. A. Birks, F. Biancalana, and P. S. J. Russell, "Supercontinuum and four-wave mixing with Q-switched pulses in endlessly single-mode photonic crystal fibres," *Opt. Express* **12**, 299-309 (2004), <http://www.opticsexpress.org/abstract.cfm?URI=OPEX-12-2-299>
 18. B. R. Washburn, S. E. Ralph, P. A. Lacourt, J. M. Dudley, W. T. Rhodes, R. S. Windeler, and S. Coen, "Tunable near-infrared femtoseconds (*??title??*)soliton generation in photonic crystal fibres," *Electron. Lett.* **37**, 1511-1512 (2001).
 19. J. H. V. Price, K. Furusawa, T. M. Monro, L. Lefort, and D. J. Richardson, "Tunable, femtoseconds pulse source operating in the range 1.06-1.33 μm based on an Yb^{3+} -doped holey fiber amplifier," *J. Opt. Soc. Am. B* **19**, 1286-1293 (2002).
-

1. Introduction

Spectral-domain optical coherence tomography (SD-OCT) makes use of low-coherence spectral interferometry to obtain cross-sectional images of a biological sample.¹⁻³ Interference fringes as a function of wavelength are measured using a broadband light source and a spectrometer based on a charge-coupled-device (CCD) camera.^{4,5} The axial reflectivity profile of a sample, or an A-line, is obtained by a discrete Fourier transform of the camera readout data. This imaging technique has recently gone through rapid technical development to demonstrate high quality imaging of biological samples with fast image acquisition time, an order of magnitude faster than state-of-the-art time-domain OCT systems.⁶⁻¹¹ The recent advancement in imaging speed may lead to the utilization of SD-OCT in a number of clinical applications in the near future.

SD-OCT systems that have been demonstrated to date utilized either a continuous-wave (cw) broad-spectrum light source, such as super luminescent diodes (SLD), or ultrashort modelocked pulses with a high repetition rate in the range of 10 - 100 MHz. In both cases, the CCD array is illuminated constantly, and therefore the exposure time of the CCD camera determines the signal acquisition time for a single A-line. A recent study¹² has shown that sample or probe motion during the A-line acquisition time can result in various undesirable artifacts such as signal fading and spatial resolution degradation. In particular, due to axial sample motion, the visibility of detected spectral fringes can diminish significantly resulting in significant image fading. Considering that cameras appropriate for SD-OCT typically provide exposures times longer than 10 μs , a solution to the fringe washout problem will be required for biomedical applications where sample and probe motion is common.¹²

In this paper, we demonstrate a technique to avoid spurious motion artifacts in SD-OCT. The technique is based on the use of single, relatively short pulse per camera exposure. The short illumination produces snap-shot axial profiles of a sample with greatly reduced motion artifacts. In addition, we extend this pulsed-source technique to a cw wavelength-swept source to gain similar benefits.

2. Principle

Figure 1 illustrates signal detection in SD-OCT for three different light sources: (a) broadband cw, (b) broadband pulsed, and (c) narrowband wavelength-swept. In the illustration, spectrally dispersed, broad-spectrum light is incident on a CCD array so that each CCD pixel receives a narrowband portion of the source light. The vertical bars (green) represent the time window during which the camera integrates photon-generated electrons. The first schematic, Fig. 1(a),

corresponds to the common implementation of SD-OCT. The operational principles of the systems corresponding to Figs. 1(b) and (c) are described in the following two sections.

2.1 Pulsed source approach

Figure 1(b) depicts a train of short broadband pulses with a repetition rate equal to the CCD readout rate. The integration time of the system in this case, is given by the pulse duration rather than the camera readout time. As a result, snap-shot A-line profiles can be obtained with freedom from sample or probe motion. This technique is conceptually similar to the use of stroboscopic illumination in photography. Although for most biomedical applications nanosecond pulses are sufficiently short to avoid motion artifacts, it is interesting to note that in principle, this approach could provide femtosecond temporal resolution A-line acquisition through the use of low-repetition mode locked lasers. The following analysis, however, pertains to an arbitrary pulsed source delivering either single bursts of short-duration broadband light or bursts comprising a brief train of mode locked pulses.

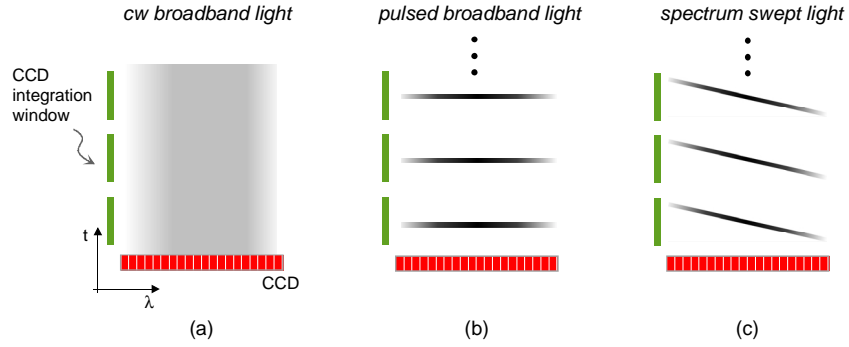


Fig. 1. Detection of (a) cw, (b) pulsed, and (c) swept light with a CCD array in a spectrometer.

In order to understand the imaging characteristics of a pulsed-source SD-OCT system, the signal-to-noise ratio (SNR) for pulsed and cw operation in the presence of axial motion was investigated. Let T_s and T_e denote the duration of the pulse and the electrical integration time of the camera, respectively. For a sample moving axially in parallel to an optical probe beam with a speed v_z , the signal power S , normalized to the signal at $v_z = 0$, is given by¹²

$$S \approx \left| \int_0^{T_e} P(t) e^{j2k_0 v_z t} dt \right|^2 / \int_0^{T_e} P(t) dt^2, \quad (1)$$

where $P(t)$ represents time-varying optical power of the pulse, and $k_0 = 2\pi/\lambda_0$ denotes the wave number corresponding to the center wavelength λ_0 . Equation 1 yields $S \approx \sin^2(k_0 \Delta z) / (k_0 \Delta z)^2$ for a square pulse and $S \approx \exp[-k_0^2 \Delta z^2 / (2 \ln 2)]$ for a Gaussian pulse with T_s as the full-width-at-half-maximum (FWHM) pulse duration, where $\Delta z = v_z T_s$ represents the total sample movement during pulse duration T_s . These expressions imply that significant signal fading occurs if the sample movement is greater than a half optical wavelength during the pulse duration. Therefore, the short pulsed technique ($T_s \ll T_e$) offers a significant advantage over the conventional cw operation in terms of motion-induced signal fading. Similarly, one can see that pulsed operation can also suppress other motion artifacts, such as spatial resolution degradation due to sample motion and transverse beam scanning.

The fundamental noise characteristics of pulsed operation are expected to be identical to those of cw operation, because the detection bandwidth is solely determined by the integration time of the camera. If both a pulsed and cw sources produce the same average optical power

and relative intensity noise (RIN), both would yield the same SNR in the limit of a stationary sample.

2.2 Swept source approach

Figure 1(c) illustrates an alternative pulsed-source SD-OCT approach that is based on a narrowband, wavelength-swept source. Since the optical spectrum is continuously changed in time, each of the CCD pixels receives its corresponding spectral component only for a short time interval. As with pulsed broad bandwidth illumination, rapidly sweeping the wavelength allows the SD-OCT signal to be free from signal fading due to fringe washout. However, unlike pulsed operation, individual “spectrum pulses” do not arrive at the CCD pixels at the same time. For a linear sweep [Fig. 2(c)], the swept operation is analogous to optical frequency domain imaging (OFDI)¹³ in which spectral fringes are measured as a function of time using a swept source and a standard photodiode. Therefore, both imaging techniques will exhibit similar motion artifacts. The motion artifacts in OFDI have been described in detail elsewhere.¹² The swept-source operation in SD-OCT, however, differs from OFDI in that it does not require a linear tuning slope or narrow instantaneous linewidth of the source because these specifications are governed by the detection spectrometer. These two distinctions are significant considering that tuning speed and power in wavelength swept lasers are often limited by constraints on linearity and instantaneous linewidth.

3. Experiment

3.1 Light sources

For proof-of-concept experiments, pulsed and wavelength-swept sources were constructed. The pulsed broadband source was realized by external time-gating of cw broadband amplified spontaneous emission (ASE) from a semiconductor optical amplifier (SOA, Philips CQF 882/e). The output of the SOA, prior to time gating, was characterized as cw un-polarized ASE centered 1.3 μm , with 7-mW total power at an injection current of 450 mA. The cw ASE was coupled to an external optical gating device comprising a polygonal mirror scanner in conjunction with a circulator. A schematic of the gating device is depicted in Fig. 2(a). The polygonal mirror had 40 facets with a facet-to-facet angle of 9 degrees. The focal lengths of the collimating (L1) and focusing (L2) lenses were chosen to be 11 and 100 mm, respectively, to obtain a duty cycle of approximately 5% in the output. Figure 3(a) shows the output pulse train measured with an InGaAs photodetector and oscilloscope (detection bandwidth = 100 MHz), as the polygon scanner was rotated at 474 revolutions per second to produce a pulse repetition rate of 18.94 kHz. The measured pulse width and corresponding duty cycle were 2.85 μs (FWHM) and 5.4%, respectively. The average output power measured with a power meter was 300 μW . Figure 3(b) shows the output spectrum measured with an optical spectrum analyzer. The spectrum was identical to that of the input ASE, with a center wavelength at 1300 nm and a FWHM of 66 nm.

Figure 2(b) depicts a schematic of the wavelength-swept laser. The laser employed the same SOA and a scanning wavelength filter based on a polygonal mirror scanner¹⁴ in a fiber-optic ring laser cavity. The scanning filter consisted of a diffraction grating (G, 830 lines per mm), two lenses in 4f configuration (L3; $f = 60$ mm, L4; $f = 63.5$ mm), and the same 40-facet polygonal mirror scanner as used for the pulsed source. The scanning filter was configured to have a free spectral range of 275 nm centered at 1320 nm wavelength, which resulted in a duty cycle of the laser output closely matched to that of the CCD camera (46%). When the pass band of the filter scans outside the gain bandwidth of the SOA, the source does not reach the lasing threshold and simply produces ASE. Figure 3(c) shows the temporal characteristics of the laser output at a sweep repetition rate of 18.94 kHz. The region where the output power varies with a Gaussian-like profile corresponds to when the source was operated above the lasing threshold. Outside this region, the output is ASE with a constant power. To determine

how much the ASE level contributed to the detected light during swept laser operation, the backward-propagating ASE power was measured by inserting a 5% tap coupler in the cavity between the filter and SOA (lower trace in Fig. 3(c), gray line). The ASE level dropped significantly during laser operation because ASE was suppressed due to gain saturation in the SOA. The laser-to-ASE ratio reached as high as 16 dB in the middle of the lasing tuning range. Horizontal bars (green) represent the integration window of the camera, which was synchronized with laser tuning. The average output power measured with a power meter was 18 mW. Figure 3(d) depicts the output spectrum measured with the optical spectrum analyzer in a peak-hold mode. In peak-hold mode, the contribution of ASE to the measurement would be negligible owing to its much lower spectral density than laser light at a given time. Therefore, the measured spectrum represents the tuning envelope of the swept laser. The tuning range was approximately 135 nm, centered at 1325 nm. The instantaneous linewidth of the swept output was approximately 0.4 nm, as determined by measuring the coherence length with a variable-delay interferometer.

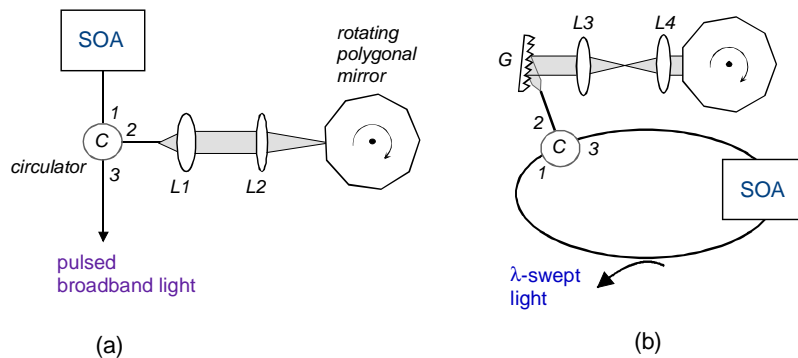


Fig. 2. Experimental configurations of (a) the pulsed ASE source and (b) wavelength-swept source.

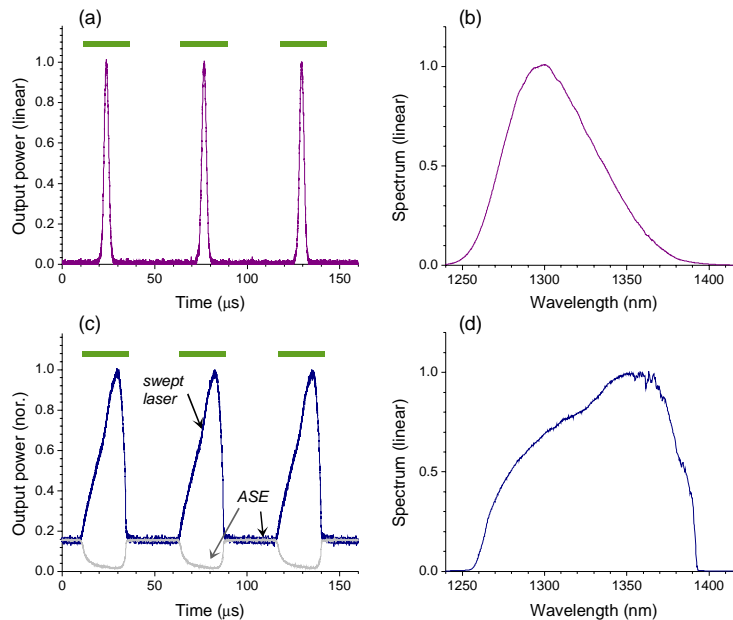


Fig. 3. Temporal and spectral output characteristics of the pulsed ASE source, (a) and (b), and the swept source, (c) and (d), respectively. The horizontal bars (green) represent the electrical integration time of the CCD camera.

3.2 OCT system

Figure 4 depicts a schematic of the SD-OCT system used in the experiment. The interferometer, probe, and detection spectrometer have been described elsewhere in detail.⁷ Briefly, the system included a circulator and a 10/90 coupler for the interferometer for efficient power utilization. A galvanometer was used in the probe to provide transverse beam scanning across a sample with a FWHM beam diameter and confocal length of 18 μm and 1.1 mm, respectively. The detection spectrometer, shown in the dash-dot box, consisted of a ruled diffraction grating with 1,200 lines per mm, focusing lens ($f = 150$ mm), and a line scan camera (LSC) with a 512-element InGaAs CCD array (Sensors Unlimited Inc., SU512LX). Polarization controllers were adjusted to maximize the fringe visibility in the CCD. A total wavelength span of 106 nm centered at 1320 nm was projected to the 512-element CCD array with a spectral resolution of 0.1 nm.

The camera readout was triggered by an external TTL signal generated from the source output. In the case of the pulsed light source, the electrical trigger pulses were generated directly from the optical pulses, as illustrated in the dotted box in Fig. 4. In the swept source case, the laser output was transmitted through a combination of a circulator and a fiber Bragg grating reflector with 0.2 nm bandwidth and 90% reflectivity (this narrowband filter arrangement is presented by a small dotted box labeled F in Fig. 4). The photodetector then detected a train of short pulses generated when the output spectrum of the laser swept through the reflection band of the Bragg grating. From the photodetector output, TTL trigger pulses were generated with adjustable phase delay.

As described earlier, both lasers were operated at a repetition rate of 18.939 kHz. This rate corresponded to the maximum readout rate of the camera. Upon receiving the trigger, the camera integrates photo-generated electrons for 24.4 μs ; in the subsequent 28.4 μs period, the integrated voltage is read out. By adjusting the phase delay in a PPL pulse generator, the integration time window of the camera was aligned to the output of the light sources, as shown in Figs. 3(a) and (c). The camera output was digitized with a 4-ch, 12-bit data acquisition board (National Instruments, NI PCI-6115) and processed in a personal computer. The data processing involves zero padding, interpolation and mapping to linear k -space, prior to a fast Fourier transform to create an image.

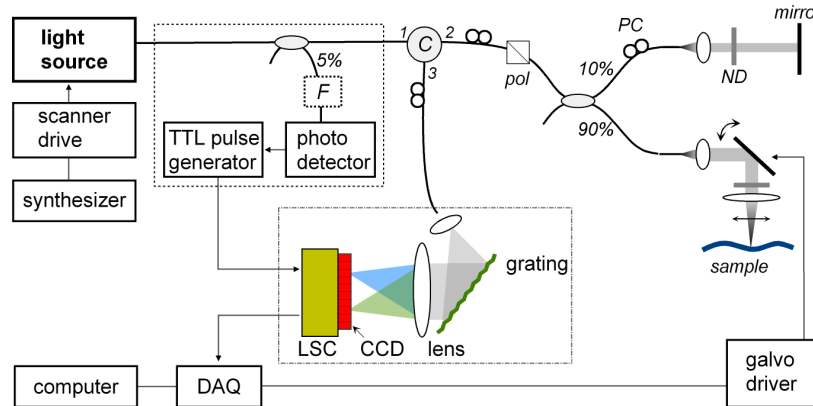


Fig. 4. Schematic of the experimental SD OCT system. F , fixed wavelength filter; pol , polarizer; PC , polarization controller; ND , neutral density filter; LSC , line scan camera; DAQ , data acquisition board.

3.3 Sample motion-induced signal fading

SD-OCT imaging was performed using three different light sources: (1) the cw ASE obtained directly from the SOA, (2) the intensity-gated ASE pulses [Fig. 2(a)], and (3) the wavelength swept laser [Fig. 2(b)]. In order to investigate motion artifacts, a sample was constructed by mounting paper on an acoustic speaker. Figure 5 compares the images obtained with three different sources. Shown on the left are OCT images acquired with cw, pulsed, and swept light, respectively, when the paper sample was kept stationary. Each image comprises 256 axial and 500 transverse pixels, spans a depth of 2.1 mm and a width of 5 mm, and was acquired over a total time period of 26.4 ms. The images were plotted using a logarithmic inverse grayscale over a dynamic range of 40 dB in reflectivity (refer to the grayscale map in Fig. 5). For each of the light sources, the optical power illuminating the sample was adjusted approximately to the same level by using neutral density filters in the probe. The offset of the grayscale map for each light source was finely adjusted so that the three static images (Fig. 5 *a*, *c*, and *e*) exhibited nearly the same contrast. Images of the axially moving sample (Fig. 5 *b*, *d*, and *f*) were acquired when the speaker was driven with a sinusoidal waveform at 80 Hz with peak-to-peak amplitude of 0.8 mm. Signal fading due to fringe washout is distinct for the case of the cw ASE source (Fig. 5*b*). Except near the peaks and valleys of the oscillation when the axial velocity was zero, the image contrast and penetration depth were noticeably degraded. In contrast, the image *d* was obtained with the pulsed source and exhibits considerably reduced image fading. Signal fading was not observed while using the wavelength swept source (Fig. 5*f*).

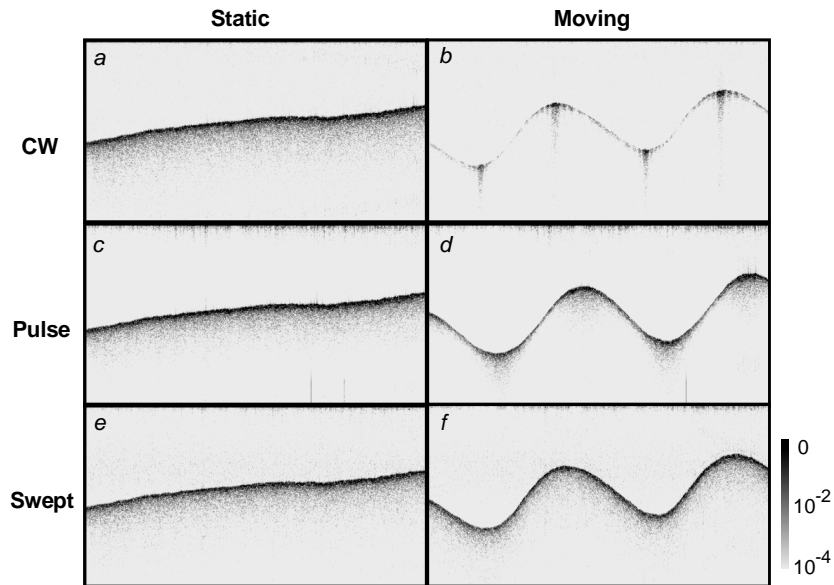


Fig. 5. SD-OCT images of a paper, acquired when the sample was static and moving at 80 Hz over 0.8 mm with three different light sources. Signal fading appears distinctly in image *b* obtained with cw ASE, but was greatly reduced with the pulsed source, *d*, and was not observed with the swept source, *f*.

To quantify the amount of signal fading, a sum of the pixel values in the unit of linear power along each A-line was obtained from the images in Fig. 5, representing a total signal power in the particular A-line. A total of 200 pixels, from the 31st to 230th elements, were considered in the summation. The results are plotted in Figs. 6 (a)-(c) corresponding, respectively, to the cw source (Figs. 5*a* and *b*), the pulsed source (Figs. 5*c* and *d*), and the swept source (Figs. 5*e* and *f*). In each graph, the integrated signal power is plotted as a function of A-line index for the

stationary-sample image (blue line) and the moving-sample image (black line). As depicted by the blue lines, the signal power for the stationary sample exhibits random fluctuation due to speckle as the probe beam is scanned across the sample with standard deviation of approximately 2 dB. The speckle-averaged mean value varies linearly over transverse locations of the sample, a variation that was attributed to the finite confocal parameter and resulting depth-dependent light collection efficiency. The signal power traces obtained from Figs. 5*b*, *d*, and *f* (black lines) clearly demonstrate the benefit of the pulsed and swept source in terms of reducing motion-induced signal fading.

The time gated pulses provided a factor 8.6 reduction in signal integration time, from 24.4 μs to 2.85 μs . For the swept source with an instantaneous linewidth of 0.4 nm, individual CCD pixels were illuminated for only 75 ns per each A-line acquisition representing a 325-fold reduction in signal integration time. Theoretical curves (red lines) based on Eq. (1) show good correspondence with the experimental results with the following exceptions. The experimental noise floor prohibited detection of signal loss greater than -14 dB; the small discrepancy between the blue and black curves in Fig. 6(c), by up to 3 dB, is attributed to the uneven probe collection efficiency at different depths of the two samples.

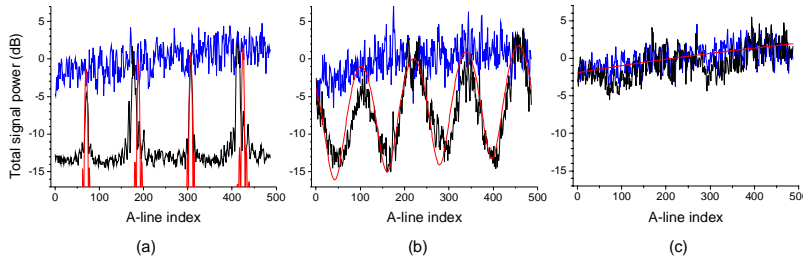


Fig. 6. Variations of total signal power, a sum of reflectivity of 256 depth points in each A-line, as a function of A-line index or time, obtained from (a) images *a* and *b* in Fig. 5, (b) *c* and *d*, (c) *e* and *f* in Fig. 5. Blue line: stationary sample, black line: moving sample, red line: theoretical curve based on Eq. (1).

Our SNR analysis indicated that the pulsed ASE source produced essentially the same noise characteristics as cw ASE of the same average optical power. However, images acquired using the wavelength swept laser exhibited a noise floor that was 10-20 dB higher, depending on depth, than that observed when using the ASE source of the same average power. We attribute this increased noise floor to the RIN of the swept laser in the frequency band from DC to 41 kHz corresponding to a reciprocal of the CCD integration time. The best sensitivity obtained with the swept source was approximately -95 dB at a reference-arm power of 1-2 μW .

3.4 Probe motion-induced signal fading

SD-OCT imaging of a human coronary artery *in vitro* was conducted by use of a fiber-optic catheter. The fiber-optic catheter comprised a graded-index lens and a 90-degree prism at its distal end and was connected to the interferometer through a high-speed rotational joint which could provide a rotational speed of up to 100 revolutions per second (rps). Figure 7 depicts the images obtained with the cw ASE source (*A* and *B*) and the swept source (*C* and *D*) at the same A-line acquisition rate of 18.94 kHz. The difference between images *A* and *B* and between *C* and *D* is the rotational speed of the catheter, which was 9.5 rps for *A* and *C*, corresponding to 2000 A-lines per image, and 37.9 rps for *B* and *D*, corresponding to 500 A-lines per image. Zero delay of the interferometer was positioned between the sample and the outer prism surface, resulting in a circular artifact superimposed on the image of the tissue (marked as *p*).

Image *A* represents a typical OCT image of a vessel. In contrast, Image *B* exhibits distinct radial streaks due to loss of signal. This image fading was attributed mainly to catheter-induced modulation in path length, increasing with the rotational speed. The path length modulation can result from three mechanisms: (1) rotational beam scanning of an off-center object inevitably results in axial path length variation of the probe beam, as if the probe was retracting or approaching to the sample; (2) the tip of a rotating catheter can wobble in a protection sheath to modulate the distance between the probe and the sample; (3) mechanical vibration from a rotation joint can modulate the length of the optical fiber inside the catheter by twist or strain. This third mechanism was thought to a dominant cause in this particular experiment, since the circle (p) corresponding to the prism surface also suffers from significant loss of contrast at the same radial locations. Figs. 7C and D depicts SD-OCT images obtained with the swept source. The signal fading is not noticeable in D, demonstrating clearly the benefit of the pulsed-source approach.

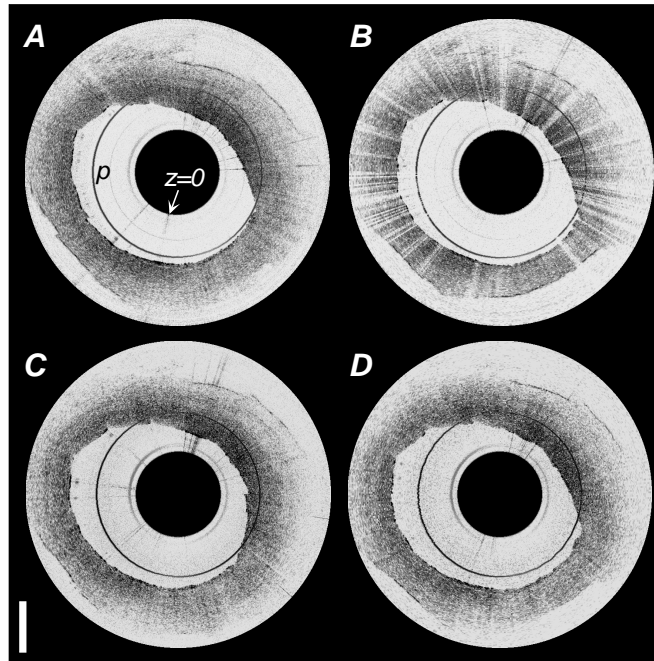


Fig. 7. SD-OCT images of a human coronary artery *in vitro* acquired with a fiber-optic rotational catheter at an A-line rate of 18.94 kHz. Each image contains 700x700 pixels. The rotation speed of the catheter and the light source that were used for each image are as follows. A; (4.5 rps, cw ASE source), B; (37.9 rps, cw ASE source), C; (4.5 rps, swept source), and C; (37.9 rps, swept source). Catheter-induced signal fading is distinct in B, however is nearly unnoticeable in D. The scale bar represents 1.0 mm.

4. Discussion

SD-OCT has been demonstrated to provide dramatic improvements in sensitivity and image acquisition rate over time-domain OCT, but is prone to signal fading and image blurring due to motion. Although a solution to this limitation would be to develop faster CCD cameras, the shortest possible integration time will be ultimately limited by the minimum detection sensitivity required for sufficient image quality. We have investigated an alternative solution based on the use of pulsed sources to provide a reduced effective integration time. Considering the challenges and expense of high-speed custom camera development, the methods described in this manuscript are particularly attractive.

As suggested by our results, multiple strategies can be applied to realize the benefit of pulsed or gated illumination. Traditional light sources have included cw SLD's, supercontinuum sources, or modelocked lasers. Each of these sources can be converted into a pulsed source by use of an external intensity modulation scheme. As an intensity modulator or switch, one may consider electro-optic or acousto-optic modulators or injection current modulation. Alternatively, CCD cameras with built-in electrical shutters may be used. This external gating approach, however, has a main drawback in that it results in a loss of optical power and therefore may degrade the detection sensitivity. However, in situations where motion causes significant signal fading through fringe washout, external gating can lead to a better sensitivity despite the loss of optical power. In other applications, however, the usable optical power in the system is often limited by the maximum permissible exposure of the sample. In this case, external gating would be an effective way to attenuate the power level entering the system from a powerful source. For example, ophthalmologic retinal imaging has been performed with SD-OCT at a wavelength of 800-nm. At this wavelength, the maximum permissible cw exposure to the eyes is limited to approximately 600-700 μ W according to American National Standards Institute (ANSI).⁸ For this application, one could gate the output from a commercially available modelocked Ti:Sapphire laser and, while still providing sufficient power to the system, reduce sensitivity to motion by more than an order of magnitude.

Instead of external gating, various power-efficient internal modulation techniques may be employed. For example, Q-switching and cavity dumping are well known techniques applicable to ultrashort pulsed lasers.¹⁵ Q-switched supercontinuum sources with repetition rates of a few to tens of kHz have been reported and may be suitable for use in SD-OCT.^{16,17} Beside the benefit of reducing motion artifacts, the reduced fringe washout of the pulsed source approach may also facilitate quadrature fringe detection based on sequential phase dithering.⁴

The use of a wavelength swept source as described in this manuscript is essentially a hybrid between OFDI and SD-OCT that may permit otherwise stringent OFDI source requirements including narrow instantaneous linewidth and tuning linearity to be relaxed. In this case, the high resolution and linearity of the spectrometer can accommodate a swept laser with a nonlinear tuning element such as a resonantly scanned Fabry-Perot filter or a tunable source based on soliton self-frequency shifting in nonlinear fibers.^{18,19} Furthermore, the relaxed requirement on the instantaneous linewidth of a swept laser may facilitate the generation of higher output powers.

In conclusion, we have described, for the first time to our knowledge, the use of a pulsed broadband source and a wavelength-swept source for SD-OCT and have demonstrated the benefit of these methods for greatly reducing motion artifacts over conventional approaches based on cw or high repetition rate pulses. Moreover, we have conducted, for the first time to our knowledge, catheter-based imaging with SD-OCT. The significant motion artifacts associated with high-speed catheter operation emphasize the benefit of the short light illumination provided by pulsed sources. We expect that the pulsed-source approach in SD-OCT may find a wide range of applications.

Acknowledgement

This research was supported in part by the National Institute of Health contracts (R01-HL70039, R01-RR019768, R33-CA110130-01), the Center for Integration of Medicine and Innovative Technology (for technical development only), and by a generous gift from Dr. and Mrs. J.S. Chen to the optical diagnostics program of the Massachusetts General Hospital Wellman Center for Photomedicine.